Poly(vinylidene fluoride)/nickel nanocomposites from semicrystalline block copolymer precursors

Voet, Vincent S. D.; Tichelaar, Martijn; Tanase, Stefania; Mittelmeijer-Hazeleger, Marjo C.; ten Brinke, Gerrit; Loos, Katja

Published in:
Nanoscale

DOI:
10.1039/c2nr32990e

Publication date:
2013

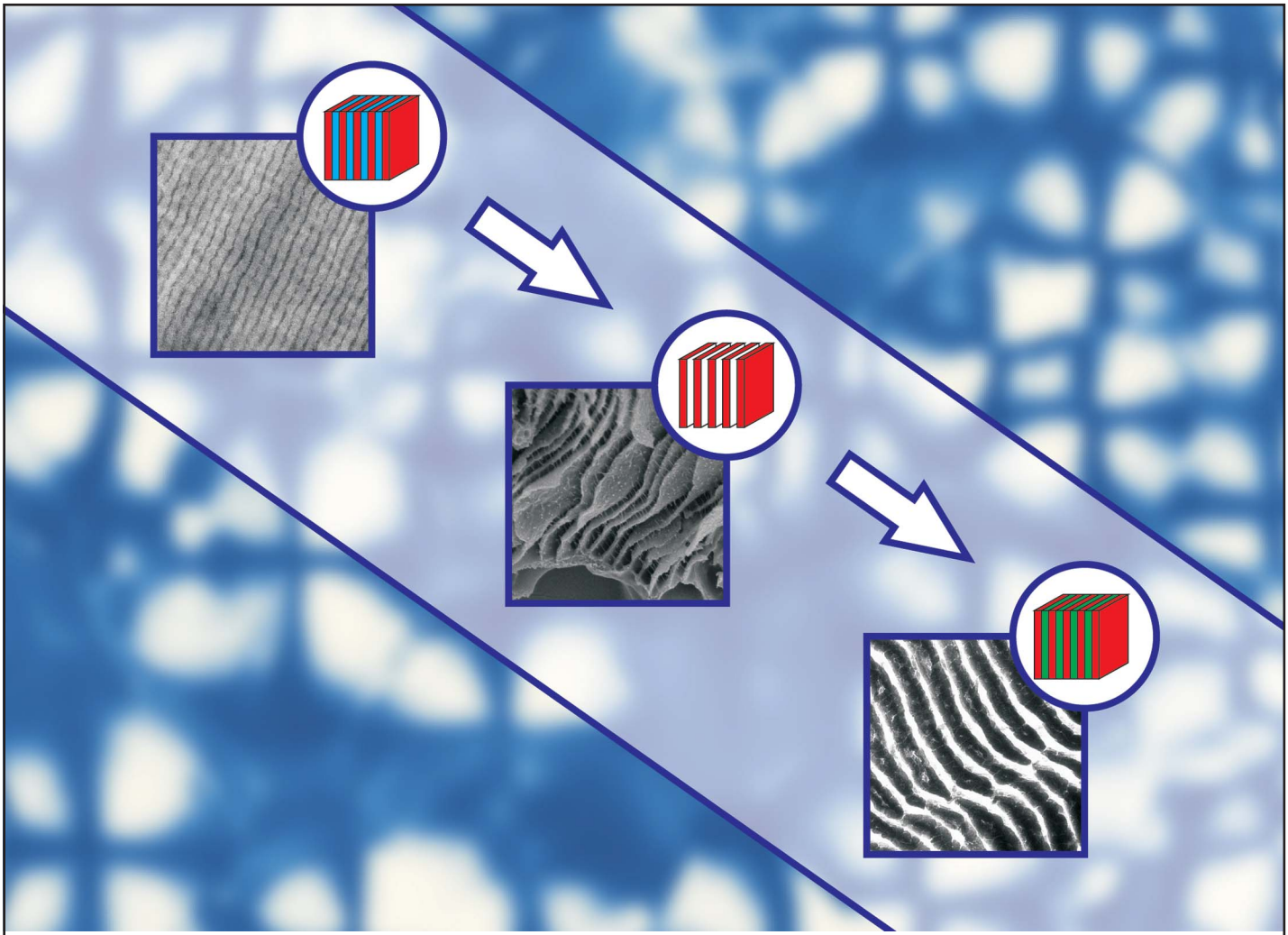

Showcasing research from the Department of Polymer Chemistry at the Zernike Institute for Advanced Materials, University of Groningen, the Netherlands.

Title: Poly(vinylidene fluoride)/nickel nanocomposites from semicrystalline block copolymer precursors

The groups of Professors Loos and ten Brinke consider the synthesis and self-assembly of block copolymers and their supramolecular complexes, together with the fabrication of functional nanocomposites and porous nanofoams from self-assembled structures. We report the preparation of nanoporous poly(vinylidene fluoride) (PVDF) and PVDF/nickel nanocomposites from triblock copolymer precursors. The lamellar morphology and β-crystalline phase are conserved during the etching procedure and nickel deposition. This research was funded by a VIDI innovational research grant of the Netherlands Organisation for Scientific Research (NWO).

As featured in:

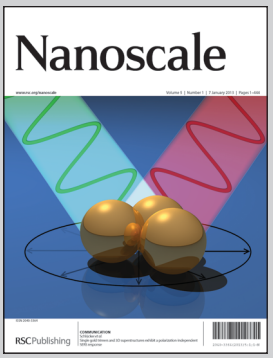

See ten Brinke and Loos *et al.*, *Nanoscale*, 2013, **5**, 184.

RSC Publishing

www.rsc.org/nanoscale

Registered Charity Number 207890

Nanoscale

RSC Publishing

PAPER

Poly(vinylidene fluoride)/nickel nanocomposites from semicrystalline block copolymer precursors†

Cite this: *Nanoscale*, 2013, 5, 184

Vincent S. D. Voet,[a] Martijn Tichelaar,[a] Stefania Tanase,[b] Marjo C. Mittelmeijer-Hazeleger,[b] Gerrit ten Brinke*[a] and Katja Loos*[a]

Received 29th September 2012
Accepted 16th October 2012

DOI: 10.1039/c2nr32990e

www.rsc.org/nanoscale

The fabrication of nanoporous poly(vinylidene fluoride) (PVDF) and PVDF/nickel nanocomposites from semicrystalline block copolymer precursors is reported. Polystyrene-*block*-poly(vinylidene fluoride)-*block*-polystyrene (PS-*b*-PVDF-*b*-PS) is prepared through functional benzoyl peroxide initiated polymerization of VDF, followed by atom transfer radical polymerization (ATRP) of styrene. The crystallization of PVDF plays a dominant role in the formation of the block copolymer structure, resulting in a spherulitic superstructure with an internal crystalline–amorphous lamellar nanostructure. The block copolymer promotes the formation of the ferroelectric β-polymorph of PVDF. Selective etching of the amorphous regions with nitric acid leads to nanoporous PVDF, which functions as a template for the generation of PVDF/Ni nanocomposites. The lamellar nanostructure and the β-crystalline phase are conserved during the etching procedure and electroless nickel deposition.

Introduction

The discovery of piezoelectricity in poly(vinylidene fluoride) (PVDF) in 1969 by Kawai[1] has stimulated extensive research in the field of ferroelectric polymers.[2–5] In contrast to ferroelectric ceramics, polymers are flexible, relatively inexpensive and processable in large area sheets and molded shapes. Consequently, PVDF and its copolymers have been commercially used in a large number of applications, *e.g.* in headphones, loudspeakers and sonar arrays.[6,7] The combination of chemical inertness, high thermal resistance and ferroelectric behavior designates PVDF as a potential material for nanotechnological applications. More specifically, porous nanomaterials composed of PVDF can be applied in mechanical actuators and separation membranes, or as ferroelectric templates for the fabrication of novel polymer nanocomposites.

Nanocomposites containing PVDF represent a new class of materials with enhanced performance and new functionalities. PVDF/clay nanocomposites have been constructed to either improve the physical properties of the polymer, or to induce the formation of the polar β-polymorph of PVDF, which is known for its ferroelectric behavior that originates from the *all-trans* chain conformation.[8,9] In addition, polymer-based multiferroic magnetoelectric nanocomposites, combining ferroelectric PVDF and a ferromagnetic phase, have attracted considerable attention in recent years.[10,11] These multiferroic composites have been found to exhibit a strain-coupled magnetoelectric effect (*i.e.* the appearance of an electric polarization upon applying a magnetic field, or the appearance of magnetization upon applying an electric field) of several orders of magnitude higher compared to the response in single-phase magnetoelectric materials. Indeed, nanocomposites composed of a piezoelectric polymer and a magnetostrictive compound, such as PVDF/Terfenol-D,[12] PVDF/Metglas[13] and PVDF/$N_{0.5}Zn_{0.5}F_2O_4$ (ref. 14) demonstrated giant magnetoelectric effects and can be potentially used in sensors and memory devices.

Block copolymers are able to microphase separate into morphologies ordered on the nanoscale (typically 10–100 nm), and their phase behavior has been studied extensively.[15–20] Block copolymers containing a degradable component provide a convenient route towards porous nanostructured materials with desired functionality and controllable pore sizes.[21–23] For example, selective removal of the cylinder-forming phase in a self-assembled block copolymer structure results in the formation of nanochannels within a polymer matrix. Etching of the so-called sacrificial block is achieved *via* several degradation techniques, *e.g.* hydrolysis,[24] UV irradiation,[25] amphiphile extraction[26,27] and reactive ion etching.[28] Recently, enhanced thermal and mechanical stability of nanoporous materials was demonstrated with the preparation of semicrystalline nanoporous polyethylene films from crystalline–amorphous polyethylene-*block*-polystyrene (PE-*b*-PS) block copolymers.[23,29] The procedure included selective etching of the amorphous PS blocks with fuming nitric acid, leading to a semicrystalline PE network with excellent mechanical strength and high flexibility.

[a]*Department of Polymer Chemistry, Zernike Institute for Advanced Materials, University of Groningen, Nijenborgh 4, 9747 AG Groningen, The Netherlands. E-mail: k.u.loos@rug.nl; g.ten.brinke@rug.nl*

[b]*Van 't Hoff Institute for Molecular Sciences, University of Amsterdam, Science Park 904, 1098 XH Amsterdam, The Netherlands*

† Electronic supplementary information (ESI) available: Additional ^{19}F-NMR, GPC and WAXS data are included. See DOI: 10.1039/c2nr32990e

Porous nanostructured materials from block copolymer precursors can be employed as templates for polymer-based nanocomposites. Electroless plating is a well-exploited technique to deposit metals such as gold and nickel on polymer substrate surfaces.[30–32] The process involves chemical reduction of metal ions and the subsequent autocatalytic deposition of the metal onto a catalytic surface. This technique allows the uniform coating onto complex shaped surfaces and inside nanostructured templates.[33] For example, electroless deposition of nickel inside a porous PS matrix, obtained *via* the selective degradation of a gyroid-forming block copolymer, gave rise to the formation of a PS/Ni nanocomposite with bicontinuous morphology.[34] Considering the ferromagnetic properties of nickel, a similar approach with PVDF-containing block copolymers will result in a PVDF/Ni nanocomposite, composed of a ferroelectric and a ferromagnetic phase.

Block copolymers with a narrow polydispersity are required to enable the self-assembly into well-ordered morphologies. The synthesis of such well-defined block copolymers requires a chain-growth mechanism with the absence of undesired transfer and termination steps. Living anionic polymerization and controlled radical polymerization are therefore suitable preparation techniques.[35] Among them, atom transfer radical polymerization (ATRP)[36] is often applied successfully.[37,38] Only a few studies however report on the synthesis of well-defined PVDF-based block copolymers, since fluoromonomers cannot be readily polymerized by living anionic polymerization[39] or controlled radical polymerization techniques.[40] Poly(vinylidene fluoride)-*block*-poly(methyl methacrylate) (PVDF-*b*-PMMA) and poly(vinylidene fluoride)-*block*-polystyrene (PVDF-*b*-PS) copolymers were prepared *via* ATRP from PVDF telomers,[41] which are prepared *via* radical telomerization of vinylidene fluoride in the presence of chloroform. Higher molecular weight fluoropolymer segments were obtained by emulsion copolymerization of VDF and hexafluoropropylene (HFP) in the presence of a halogen chain transfer agent.[42,43] The resulting PVDF-*co*-PHFP copolymers, with molecular weights up to 25 kg mol^{-1}, were used as efficient macroinitiators for the ATRP of styrene or methyl methacrylate to prepare diblock copolymers. A similar strategy was adopted to produce PS-*b*-PVDF-*b*-PS triblock copolymers.[44] The PVDF segment was prepared *via* radical polymerization initiated by chloromethyl benzoyl peroxide,[45] and the chain-end-functionalized PVDF subsequently initiated the ATRP of styrene to generate triblock copolymers. Recently, block copolymers consisting of PVDF and poly(aromatic sulfonates) were synthesized,[46] combining two CRP techniques, *i.e.* iodine transfer polymerization (ITP) and ATRP.

The incorporation of crystallizable blocks, such as poly(vinylidene fluoride), may completely change the block copolymer morphology.[18,47–49] The structure development in these crystalline–amorphous (or semicrystalline) block copolymers is controlled by two competing self-organizing mechanisms: crystallization and microphase separation driven by block incompatibility. This allows the formation of different morphologies, depending on the segregation strength, the crystallization temperature (T_c), the glass transition temperature of the amorphous block (T_g) and the order–disorder transition temperature (T_{ODT}). When the block incompatibility is small ($T_{ODT} < T_c$) and the amorphous matrix is rubbery during crystallization ($T_g < T_c$), crystallization proceeds from a homogeneous melt. Consequently, alternating crystalline–amorphous lamellar microdomains within a spherulitic superstructure are observed for a wide range of copolymer compositions.[50,51]

Despite the successful synthesis of PVDF-containing block copolymers, the phase behavior of such crystalline–amorphous block copolymers has hardly been studied, even though the resulting ordered nanostructured block copolymer systems may facilitate the preparation of nanoporous PVDF templates, and subsequently PVDF/Ni nanocomposites. In this study, we report the synthesis of semicrystalline polystyrene-*block*-poly(vinylidene fluoride)-*block*-polystyrene and investigate the self-assembled block copolymer structure. Additionally, we demonstrate the selective removal of amorphous polystyrene blocks, followed by electroless nickel plating of the resulting nanoporous PVDF matrix, to generate a PVDF/Ni composite.

Experimental

Materials

Styrene (S, Acros, 99%) was dried overnight in a nitrogen atmosphere over CaH_2 and condensed at room temperature (10^{-6} mbar). Oxalyl chloride (Acros, 98%), 4-(chloromethyl) benzoic acid (Acros, 98%), lithium peroxide (Li_2O_2, Acros, 95%), vinylidene fluoride (VDF, Synquest Labs, 98%), copper(I) chloride (CuCl, Acros, 99.99%), 1,1,4,7,7-pentamethyldiethylenetriamine (PMDETA, Acros, 99+%), nitric acid (Merck, 99.5+%), tin chloride ($SnCl_2$, Acros, 98%), hydrochloric acid (HCl, Merck, 37%), palladium chloride ($PdCl_2$, Aldrich, 60% Pd basis), nickel sulfate ($NiSO_4 \cdot H_2O_6$, Aldrich, 99%), citric acid trisodium salt ($Na_3C_6H_5O_7$, Aldrich, 98%), lactic acid (SAFC, 85%), borane dimethylamine complex (DMAB, Aldrich, 97%) and ammonium hydroxide (NH_4OH, Aldrich, 29% NH_3 basis) were used as received. All solvents used were of analytical grade.

Synthesis of 4-(chloromethyl)benzoyl peroxide

Oxalyl chloride (5.4 mL, 63 mmol) and a few drops of anhydrous DMF were added to a stirred solution of 4-(chloromethyl)benzoic acid (10 g, 59 mmol) in 50 mL of anhydrous DCM at 0 °C. After reacting for 2 h at room temperature, the solvent was removed by rotary evaporation. The remaining yellow residue was immediately dissolved in 100 mL *n*-hexane–EtOH (1 : 1). The resulting solution was slowly added *via* a droplet funnel to a rapidly stirred 20 mL aqueous solution of Li_2O_2 (3.5 g, 75 mmol) at 0 °C. After reacting for 2 h at room temperature, the reaction mixture was diluted with 250 mL chloroform and washed twice with 100 mL H_2O. The aqueous phase was extracted twice with 50 mL chloroform. The combined organic phases were dried over $MgSO_4$ and chloroform was subsequently removed by rotary evaporation. The remaining white solid was recrystallized from chloroform, yielding white needle-shaped crystals. ^{1}H-NMR (400 MHz, DMSO-d_6, δ): 8.12 (d, 4H, –Ar*H*), 7.76 (d, 4H, –Ar*H*), 4.95 (s, 4H, –CH_2Cl).

Synthesis of chlorine-terminated PVDF

A typical procedure for the polymerization of vinylidene fluoride is as follows. A solution of 4-(chloromethyl)benzoyl peroxide (1.5 g, 4.5 mmol) in 300 mL of anhydrous acetonitrile was added to a pressure reactor (Parr Instruments, model 4568). The vessel was closed and purged with nitrogen for 30 min to degas the mixture. Subsequently, the reactor was charged with 20 bar of VDF, heated to 90 °C and stirred at 700 rpm. After reacting for 15 min, the vessel was cooled down to room temperature and depressurized. The reaction mixture was cooled to 0 °C, and the precipitate was collected by filtration. The remaining solid was washed with acetonitrile and chloroform, and finally dried in vacuum at room temperature to yield a white solid. ^{1}H-NMR (400 MHz, DMSO-d_6, δ): 8.01 (d, –Ar*H*), 7.61 (d, –Ar*H*), 4.84 (s, –CH_2Cl), 4.64 (m, –COOCH_2CF$_2$–), 2.87 (t, –CF$_2$CH_2–CF$_2$CH$_2$–, head-to-tail), 2.23 (t, –CF$_2$CH_2–CH$_2$CF$_2$–, tail-to-tail). ^{19}F-NMR (400 MHz, DMSO-d_6, δ): −92.0 (–CH$_2$CF$_2$–CH$_2$CF_2–CH$_2$CF$_2$–, head-to-tail), −94.8 (–CH$_2$CF$_2$–CF$_2$CH$_2$–CH$_2$CF_2–CH$_2$CF$_2$–), −113.8 (–CH$_2$CF$_2$–CH$_2$CF_2–CF$_2$CH$_2$–), −116.1 (–CH$_2$CF$_2$–CF_2CH$_2$–CH$_2$CF$_2$–).

Synthesis of PS-*b*-PVDF-*b*-PS

A typical procedure for the atom transfer radical polymerization of styrene is as follows. Chlorine-terminated PVDF (0.39 g, 0.025 mmol) and CuCl (50 mg, 0.50 mmol) were added to a dried Schlenk tube sealed with a rubber septum, followed by a degassing procedure (*i.e.* evacuating and backfilling three times with nitrogen). 5.0 mL of anhydrous DMF was added *via* a degassed syringe to dissolve the PVDF macroinitiator. PMDETA (0.31 mL, 1.5 mmol) was added *via* a degassed syringe and the solution was stirred for at least 10 min to let the dark green colored catalyst–ligand complex form. Subsequently, styrene (2.68 mL, 22.5 mmol) was added *via* a degassed syringe, and the reaction mixture was immediately subjected to at least four freeze–pump–thaw cycles to degas. After reacting at 110 °C for a desired amount of time, the dark-brown mixture was cooled down to room temperature using a water bath and subsequently precipitated in MeOH–H_2O (100 mL, 1 : 1). The solid was collected by filtration and washed with MeOH–H_2O (1 : 1), methanol and *n*-hexane. Reprecipitation was carried out from DMF in MeOH–H_2O (1 : 1), and the collected off-white solid was dried in vacuum at 40 °C. (400 MHz, acetone-d_6, δ): 7.29 (m, –Ar*H*), 6.86 (m, –Ar*H*), 3.18 (t, –CF$_2$CH_2–CF$_2$CH$_2$–, head-to-tail), 2.53 (t, –CF$_2$CH_2–CH$_2$CF$_2$–, tail-to-tail), 2.12 (m, –CH$_2$C*H*Ph–), 1.79 (m, –CH_2CHPh–).

Preparation of block copolymer films

Solvent annealing was applied to obtain a phase separated block copolymer nanostructure. A 1.5% w/w solution of PS-*b*-PVDF-*b*-PS in DMF was stirred for at least 2 h at room temperature and the solution was subsequently poured in a glass Petri dish. The solvent was allowed to slowly evaporate at 45 °C and the film was annealed in a saturated solvent vapor for at least one week, yielding a slightly yellow transparent film.

Preparation of nanoporous films

Acid etching was employed to selectively remove polystyrene from the block copolymer structure. The PS-*b*-PVDF-*b*-PS film was submerged in 10 mL of fuming nitric acid. After 5 min, the nitric acid was decanted, and the treated film was washed with H_2O and methanol. The resulting white film was dried in vacuum at room temperature.

Preparation of PVDF/Ni nanocomposites

Electroless metal plating was employed for nickel deposition onto the polymer substrate. For surface sensitization, the nanoporous template was immersed into a solution of $SnCl_2$ (0.1 M) and HCl (0.1 M) in MeOH–H_2O (1 : 1) for 1 h, and the surface of the pores adsorbed Sn^{2+}. The sensitized film was rinsed with MeOH–H_2O (1 : 1) and soaked into a solution of $PdCl_2$ (1.4 mM) and HCl (0.25 M) in MeOH–H_2O (1 : 1) for 1 h. The surface was activated by a redox reaction ($Sn^{2+} + Pd^{2+} \rightarrow Sn^{4+} + Pd^0$) to exchange Sn^{2+} adsorbed on the surface into Pd^0. After rinsing with MeOH–H_2O (1 : 1), the activated film was immersed into an aqueous electroless nickel plating bath composed of $NiSO_4 \cdot H_2O_6$ (40 g L^{-1}), $Na_3C_6H_5O_7$ (20 g L^{-1}), lactic acid (10 g L^{-1}) and DMAB (1 g L^{-1}). The metallic palladium functions as a catalyst for the reduction of Ni^{2+}. The pH of the nickel bath was adjusted to 7 using an aqueous solution of NH_4OH (1.0 M), and the plating was performed at room temperature for 1 h. The nickel plated film was rinsed with H_2O and dried in vacuum at room temperature.

Characterization

^{1}H and ^{19}F nuclear magnetic resonance (^{1}H-NMR and ^{19}F-NMR) spectra were recorded on a 400 MHz Varian VXR operating at room temperature. Gel permeation chromatography (GPC) was performed in DMF (1 mL min^{-1}) with 0.01 M LiBr on a Viscotek GPCMAX equipped with model 302 TDA detectors, using two columns (PSS-Gram-1000/30, 10 μ 30 cm). Molecular weights were calculated relative to polystyrene according to universal calibration using narrow disperse standards (Polymer Laboratories). Differential scanning calorimetry (DSC) was carried out using a TA Instruments Q1000 in a nitrogen atmosphere and with a heating/cooling rate of 10 °C min^{-1}. Polarized optical microscopy (POM) was conducted on a Zeiss Axiophot. Wide-angle X-ray scattering (WAXS) and Small-angle X-ray scattering (SAXS) were performed at the Dutch-Belgium Beamline (DUBBLE) station BM26B of the European Synchrotron Radiation Facility (ESRF) in Grenoble, France. The sample-detector distance of the SAXS set-up was *ca.* 6 m, while the X-ray wavelength was 1.03 Å. The scattering vector q is defined as $q = 4\pi/\lambda \sin\theta$ with 2θ being the scattering angle. The patterns were collected at room temperature. Transmission electron microscopy (TEM) was carried out on a Philips CM12 transmission electron microscope operating at an accelerating voltage of 120 kV. TEM samples were prepared as follows: ultrathin sections (about 80 nm) of a solvent-cast block copolymer film embedded in the epoxy resin (Epofix, Electron Microscopy Sciences) were microtomed using a Leica Ultracut

UCT-ultramicrotome equipped with a 35° Diatome diamond knife at room temperature, and subsequently placed on copper grids. Scanning electron microscopy (SEM) was carried out on a JEOL 6320F field microscope operating at 3 kV. Prior to imaging, the specimens were coated with 6 nm Pt/Pd (80 : 20). Energy-dispersive X-ray (EDX) spectroscopy was performed on a Philips XL-30 environmental scanning electron microscope. Surface area measurements were performed by the BET method using N_2 at 77 K on a Thermo Scientific Surfer instrument. The samples were dried in vacuum (10^{-3} mbar) for 24 h at 100 °C prior to the measurement. The pore size distribution was determined by mercury porosimetry, using a Thermo Fischer Scientific mercury porosimeter (Pascal 440 type).

Results and discussion

Synthesis

PS-*b*-PVDF-*b*-PS triblock copolymers were prepared *via* functionalized benzoyl peroxide initiated polymerization of vinylidene fluoride, followed by ATRP of styrene from the resulting PVDF macroinitiator (Scheme 1).

Functionalized benzoyl peroxides have demonstrated to act as effective initiators for the preparation of poly(vinylidene fluoride) and other fluoropolymers.[44,45] Both ^{1}H-NMR (Fig. 1a) and ^{19}F-NMR (Fig. S1†) demonstrate the characteristic signals (assigned in the Experimental section) for both head-to-tail and tail-to-tail structures of VDF sequences, indicating the successful synthesis of PVDF. Resonances due to unsaturated bonds are not observed in the ^{1}H-NMR spectrum, which implies the absence of disproportionation as a termination mechanism during the radical polymerization of VDF.[52] Therefore, propagating radicals are only consumed through recombination or termination with primary radicals, resulting in well-defined phenylmethyl chlorine end-groups (8.01, 7.61 and 4.84 ppm). The presence of $-CH_2-CF_2H$ (6.33 ppm) and $-CF_2-CH_3$ (1.76 ppm) end-groups in small traces can be attributed to chain transfer reactions, such as intramolecular backbiting giving rise to short chain branches.[53]

A library of end-functionalized PVDF macroinitiators has been prepared (Table 1), and their molecular weight and molar mass distribution was determined by GPC (Fig. S2†). In contrast to the free radical polymerization of hydrocarbon alkenes, where termination through combination and disproportionation leads to broad molecular weight distributions, the benzoyl peroxide initiated polymerization of vinylidene fluoride results in reasonably narrow dispersities in the range of 1.2–1.4. Adjusting

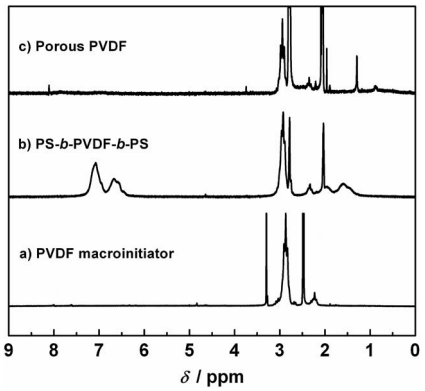

Fig. 1 ^{1}H-NMR spectra of (a) chlorine-terminated PVDF in DMSO-d_6, (b) PS-*b*-PVDF-*b*-PS triblock copolymer in acetone-d_6 and (c) nanoporous PVDF in acetone-d_6.

Table 1 Conditions and characteristics of PVDF macroinitiators

Entry	$[I]_0$ (mM)	T (°C)	p_0 (bar)	$M_{n,PVDF}$[a] (kg mol^{-1})	PDI[a]
A	5.00	90	20	16.1	1.28
B	15.0	90	20	15.7	1.29
C	50.0	90	20	11.8	1.36
D	5.00	70	20	22.1	1.38
E	5.00	110	20	13.6	1.30
F	5.00	90	10	9.3	1.20

[a] Determined by GPC in DMF.

reaction parameters such as the initial initiator concentration ($[I]_0$), temperature (T) and initial pressure (p_0) renders the possibility to alter the number average molecular weight ($M_{n,PVDF}$) and polydispersity index (PDI) of the PVDF macroinitiators.

Due to the presence of phenylmethyl chlorine end-groups and the reasonably narrow dispersity, the PVDF homopolymers are suitable to be employed as macroinitiators in the ATRP of styrene. Five block copolymers, having PS weight fractions ranging from 0.29 to 0.58 (Table 2), were prepared through ATRP with CuCl/PMDETA as the catalyst–ligand complex and PVDF B (Table 1) as the macroinitiator. The monomer conversion was determined from ^{1}H-NMR spectra of the reaction mixture by comparing the integrals of styrene (5.80 ppm, 5.23 ppm) and polystyrene (7.29–6.86 ppm). Attempts to characterize the molecular weight using GPC in DMF were unsuccessful, due to aggregation of the block copolymers. However, by comparing the integrals of PS (7.29–6.86 ppm) and PVDF (3.18 ppm, 2.53 ppm), the molecular weight ($M_{n,PS}$) and weight

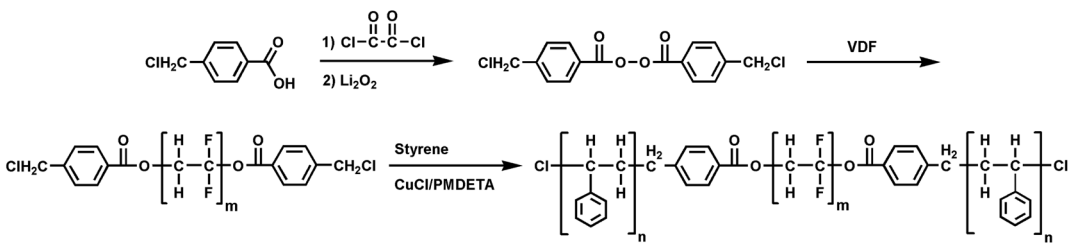

Scheme 1 Synthesis route towards the 4-(chloromethyl)benzoyl peroxide initiator, chlorine-terminated PVDF macroinitiator and PS-*b*-PVDF-*b*-PS triblock copolymer.

Table 2 Conditions[a] and characteristics of PS-*b*-PVDF-*b*-PS

Entry	t (h)	Conv[b] (%)	$M_{n,PS}$[c] (kg mol^{-1})	f_{PS}[c]
1	0.75	7.0	6.2	0.29
2	2.0	10	10.2	0.39
3	4.0	13	11.2	0.42
4	8.0	20	15.6	0.50
5	22	26	21.4	0.58

[a] [PVDF B] = 5 mM; [PMDETA] = 3[CuCl] = 0.3 M; [S] = 4.5 M. [b] Determined by ^{1}H-NMR of the reaction mixture. [c] Determined by ^{1}H-NMR of the precipitated product.

fraction (f_{PS}) were calculated from ^{1}H-NMR spectra of the precipitated product (Fig. 1b), using the predetermined $M_{n,PVDF}$ from the GPC data.

In addition, DSC analysis has been performed to study the thermal behavior of the PVDF macroinitiator and the PVDF-based triblock copolymer. The double melting endotherm around 168 °C (Fig. 2a), observed for the melting of PVDF crystals, is ascribed to melting, recrystallization and remelting during the DSC heating process,[54] which is a common phenomenon in many semicrystalline polymers. The heat flow curve of the triblock copolymer (Fig. 2b) reveals the glass transition temperature of PS segments at 106 °C, indicating phase separation between the PVDF and PS blocks.

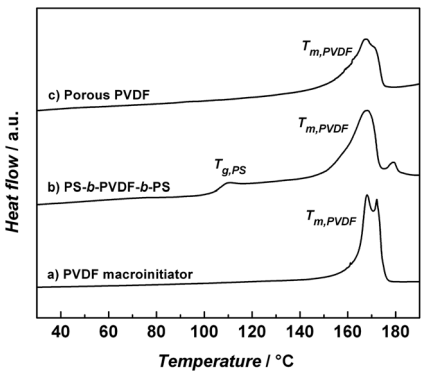

Fig. 2 DSC curves of (a) chlorine-terminated PVDF, (b) PS-*b*-PVDF-*b*-PS triblock copolymer and (c) nanoporous PVDF.

Kinetic analysis has been employed to investigate the controlled behavior of the atom transfer radical polymerization (Fig. 3). The semilogarithmic plot of conversion *versus* time suggests that the contribution of termination reactions is minimal. Furthermore, the linear relationship between M_n and monomer conversion implies that the chlorine-terminated PVDF indeed initiates a controlled radical polymerization of styrene.

Block copolymer structure

The Flory–Huggins interaction parameter between poly(vinylidene fluoride) and polystyrene has been the subject of various publications,[55,56] and values of $\chi_{VDF,S} \leq 0.021$ have been reported. Considering the chain length of the prepared triblock copolymers, this leads to values of $\chi N < 10$ below the critical value for block copolymer microphase separation to occur. Moreover, the crystallization temperature of PVDF ($T_c = 143$ °C) exceeds the glass transition of the amorphous PS ($T_g = 106$ °C). Hence, the block incompatibility is small and the amorphous matrix is rubbery during crystallization. Consequently, crystallization is expected to be the dominating self-organizing mechanism.

The morphology of the synthesized PS-*b*-PVDF-*b*-PS films, cast from DMF solution, has been examined both at the microscale (POM, SEM) and the nanoscale (TEM, SAXS). Polarized optical microscopy reveals spherulites in all triblock copolymer films (PS-*b*-PVDF-*b*-PS 1–5), with diameters of 50–80 μm (Fig. 4a). Furthermore, the microstructure of the films was confirmed by SEM images (Fig. 4b). The observed spherulitic superstructure suggests the strong influence of PVDF crystallization on the morphology.

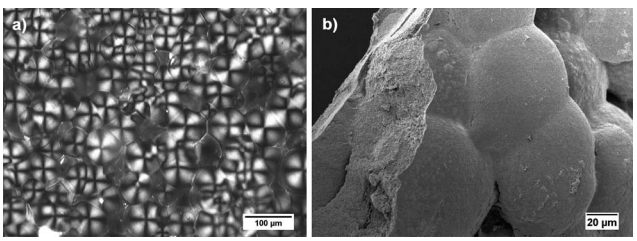

Fig. 4 (a) POM image and (b) SEM image of the spherulitic structure in PS-*b*-PVDF-*b*-PS 3 films.

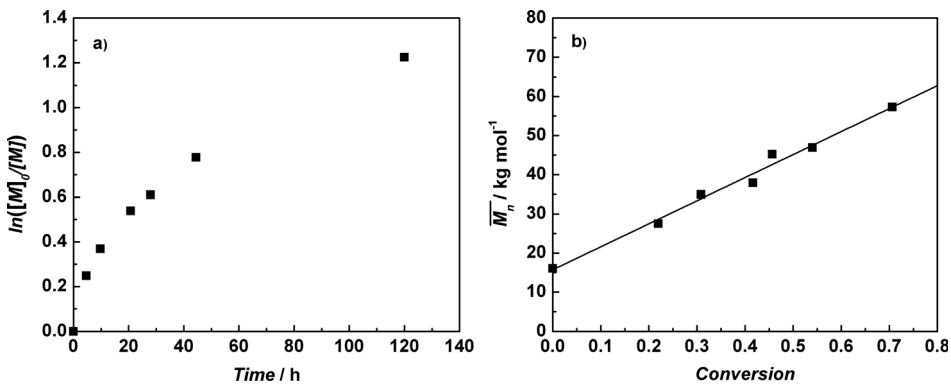

Fig. 3 (a) Kinetic plot and (b) linear dependence of the molecular weight on the monomer conversion.

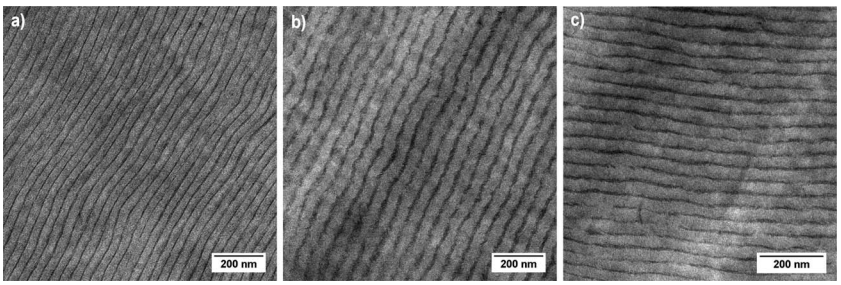

Fig. 5 TEM images of alternating crystalline–amorphous lamellae in (a) PS-*b*-PVDF-*b*-PS 2, (b) PS-*b*-PVDF-*b*-PS 3 and (c) PS-*b*-PVDF-*b*-PS 4.

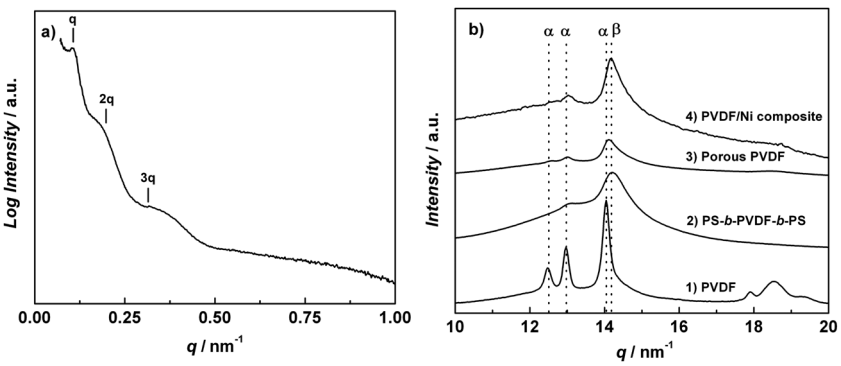

Fig. 6 (a) SAXS pattern of PS-*b*-PVDF-*b*-PS 3 and (b) WAXS pattern of (1) chlorine-terminated PVDF, (2) PS-*b*-PVDF-*b*-PS triblock copolymer, (3) nanoporous PVDF and (4) PVDF/Ni nanocomposite.

TEM measurements of the triblock copolymer films reveal a lamellar nanostructure inside the spherulitic microstructure for all copolymer compositions ($f_{PS} = 0.29$–0.58). Fig. 5 displays the TEM images of PS-*b*-PVDF-*b*-PS 2, 3 and 4. No staining has been applied to the microtomed sections prior to imaging. Therefore, we suggest that the obtained contrast arises from electron dense (dark) crystalline layers alternated by less electron dense (light) amorphous layers. Since poly(vinylidene fluoride) typically demonstrates 50–70% crystallinity according to DSC, the amorphous regions consist of PS and amorphous PVDF, which explains their larger volume compared to the crystalline regions. The alternating crystalline–amorphous lamellar nanostructure within the spherulitic superstructure confirms the dominant role of crystallization during structure formation.

The alternating lamellar morphology observed with TEM was confirmed by small-angle X-ray measurements. The SAXS intensity profile of PS-*b*-PVDF-*b*-PS 3 (Fig. 6a) demonstrates a diffraction pattern with a q ratio of 1 : 2 : 3, indicative for a lamellar nanostructure. The characteristic domain spacing, calculated from the value of the first-order reflection $q^* = 0.105\ nm^{-1}$, satisfies 60 nm, and corresponds to the length scale observed with TEM.

The crystal structure of PVDF and PVDF-containing block copolymers has been investigated by wide-angle X-ray scattering. The WAXS pattern of the PVDF macroinitiator (Fig. 6b1) reveals diffractions at $q = 12.5\ nm^{-1}$ (0.50 nm), $13.0\ nm^{-1}$ (0.48 nm) and $14.0\ nm^{-1}$ (0.45 nm). The peak positions correspond respectively to the (100), (020) and (110) α-crystal planes,[8,9] and the crystalline phase can be identified as predominantly the α-polymorph. However, the scattering pattern of PS-*b*-PVDF-*b*-PS (Fig. 6b2) demonstrates a diffraction peak at $q = 14.2\ nm^{-1}$ (0.44 nm) that arises from both (110) and (200) β-crystal planes. This peak is overlapping the broad amorphous halo, indicating a decrease of crystallinity compared to the PVDF homopolymer. The block copolymer thus promotes the formation of the polar β-polymorph of PVDF. Supposedly, the PS domains stimulate the nucleation in *all-trans* conformation, followed by the growth of nuclei, resulting in the β-crystalline phase.

Nanoporous template

The selective removal of polystyrene from the block copolymer nanostructure provides a convenient route towards porous poly(vinylidene fluoride). Fuming nitric acid etching has been applied as a facile method to selectively degrade the amorphous domains. The treated films, obtained after this etching procedure, were subjected to ^{1}H-NMR and thermal analysis. The ^{1}H-NMR spectrum demonstrates the complete removal of PS, since both the aromatic and aliphatic resonances are absent (Fig. 1c). Moreover, the PVDF signals at 3.18 (head-to-tail) and 2.53 ppm (tail-to-tail) remain, demonstrating that PVDF survived the strong acidic conditions during the etching treatment. In fact, the spectrum looks similar to the ^{1}H-NMR spectrum of the initial PVDF macroinitiator (Fig. 1a). Thermal analysis supports these findings. After the acid etching, the glass transition of polystyrene disappears (Fig. 2c), while the melting endotherm of PVDF remains.

To study the bulk morphology, the etched films were cleaved and investigated by scanning electron microscopy. As displayed in Fig. 7, a porous nanostructure is clearly revealed. The

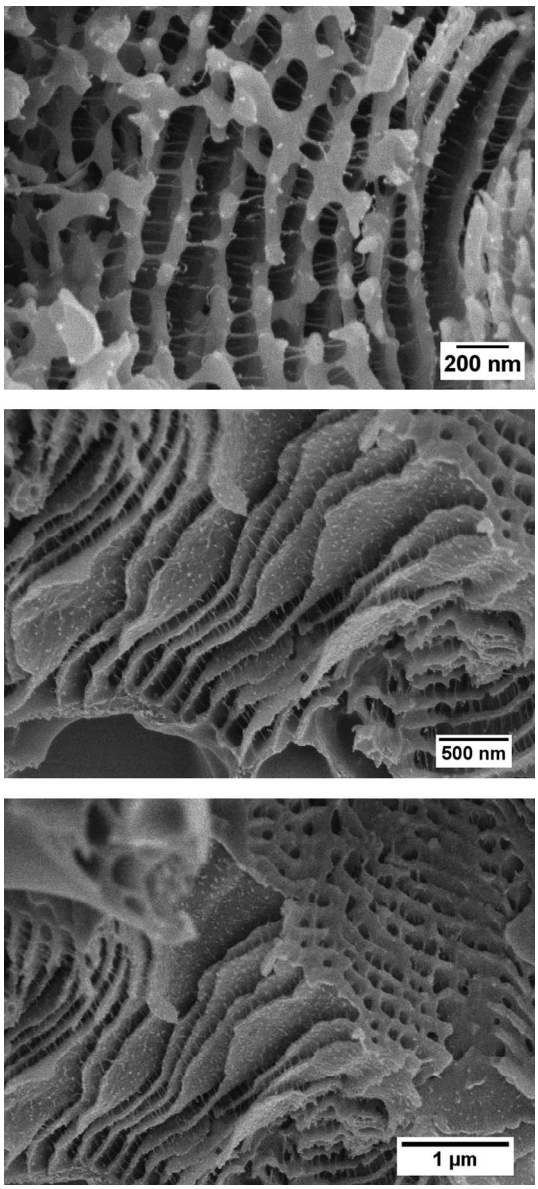

Fig. 7 SEM images of the PVDF template with a porous semicrystalline lamellar matrix, obtained after acid etching of the PS-*b*-PVDF-*b*-PS 3 film.

amorphous regions were successfully removed, resulting in a nanoporous matrix of PVDF. The lamellar morphology, originating from the block copolymer self-assembly (Fig. 5), is retained. In addition, many fibrils that bridge the crystalline lamellae are observed. Generally, a lamellar matrix is not able to support the resultant nanoporous structure after selective removal of one component, leading to a collapse of the lamellar domains.[57] However, the PVDF lamellae are confined inside a three dimensional spherulitic superstructure. Together with the high mechanical strength of the crystalline matrix, this prevents the collapse and results in a stable nanoporous structure, even with the large empty space present within the films.

Nitrogen adsorption measurements were performed to determine the surface area, evaluated by the BET method. The calculated specific surface area of the PVDF matrix is 14 $m^2\ g^{-1}$. The porosity of the template was also clearly confirmed by

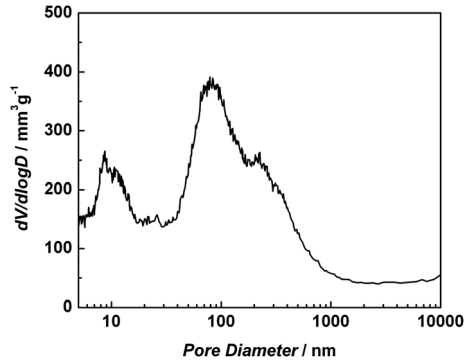

Fig. 8 Pore size distribution for nanoporous PVDF, calculated from mercury porosimetry measurements.

mercury porosimetry measurements. The pore sizes demonstrate a bimodal distribution (Fig. 8), with maxima at 10 and 85 nm, in accordance with the length scale of the nanostructure observed with SEM.

The wide-angle X-ray scattering pattern of the nanoporous template (Fig. 6b3) is similar to the pattern of the PS-*b*-PVDF-*b*-PS block copolymer, demonstrating that the β-crystalline structure was conserved during the selective degradation procedure. The WAXS data reveal a diffraction at $q = 14.2\ nm^{-1}$ (0.44 nm), corresponding to the (110)/(200) β-crystal planes. In addition, the absence of the amorphous halo (*i.e.* the increase in crystallinity) confirms the removal of amorphous polystyrene during etching.

Polymer/nickel nanocomposite

Electroless metal plating has been employed to insert nickel inside the pores of the PVDF matrix. The affinity between the plating solution and the substrate surface is an important factor for the successful metal deposition. Therefore, considering the hydrophobic nature of PVDF (contact angle on water is 82°),[58] both sensitization and activation steps of the plating procedure were performed in a MeOH–H_2O mixture in order to completely wet the surface of the pores.

TEM images of the electroless plated films (Fig. 9) demonstrate the successful deposition of the metal inside the nanoporous PVDF. Nickel penetrated the pores in the polymer matrix, resulting in a PVDF/Ni nanocomposite. No staining has been applied

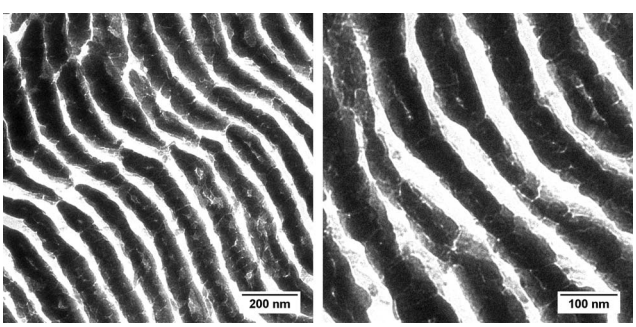

Fig. 9 TEM images of the PVDF/Ni nanocomposite with a lamellar morphology, obtained after nickel plating of the nanoporous template.

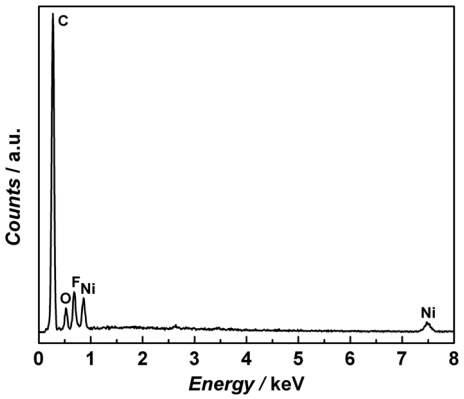

Fig. 10 EDX spectrum of the PVDF/Ni nanocomposite.

prior to TEM imaging, and the strong contrast arises from the electron dense nickel layers (black) and the less electron dense polymer layers (white). The lamellar morphology of the porous template (Fig. 7), originating from the block copolymer phase separation (Fig. 5), is clearly preserved. The electroless deposition of nickel on the PVDF matrix results in an intimate contact between the polymer and the metal phase. The PVDF/Ni composite is therefore a promising nanomaterial, since strain-coupled multiferroic composites require such an intimate contact between the piezoelectric and the magnetostrictive phase.[59]

The WAXS pattern of the PVDF/Ni nanocomposite (Fig. 6b4) is comparable to the pattern of the block copolymer and the porous template, demonstrating the presence of the β-polymorph of PVDF. This suggests that the crystalline phase of the block copolymer film is preserved during both the acid etching and electroless nickel deposition.

To study the chemical composition of the PVDF/Ni composite, the plated films were cleaved and investigated by energy-dispersive X-ray spectroscopy. Fig. 10 displays the EDX spectrum of a cross-section. Both carbon (0.28 keV) and fluorine (0.68 keV) peaks represent poly(vinylidene fluoride) in the composite, while the signals at 0.85 and 7.48 keV correspond to nickel. The presence of oxygen in the spectrum indicates the oxidation of nickel when the composite is stored in air. In addition, the complete WAXS pattern of the nanocomposite (Fig. S3†) confirms the presence of nickel, given the observed diffractions at higher q values.

Conclusion

PS-*b*-PVDF-*b*-PS block copolymers have been used as precursors for the fabrication of nanoporous PVDF and PVDF/Ni nanocomposites. First, the triblock copolymers were successfully synthesized *via* a two-step synthesis method, involving functional benzoyl peroxide initiated polymerization of VDF, followed by ATRP of styrene from the resulting macroinitiator. Kinetic analysis demonstrated the controlled behavior of the atom transfer radical polymerization.

The morphology of the semicrystalline block copolymers has been investigated, and revealed an alternating crystalline–amorphous lamellar nanostructure inside a spherulitic superstructure for a range of block copolymer compositions (f_{PS} = 0.29–0.58), confirming the dominant role of crystallization in structure formation. In addition, the β-polymorph has been detected within the block copolymer crystal structure, potentially due to the PS domains that stimulate the nucleation of the *all-trans* chain conformation of PVDF.

The amorphous PS block has been removed selectively by applying a facile chemical etching method with fuming nitric acid, leading to a nanoporous PVDF matrix. The use of semicrystalline block copolymers as precursors for these materials will enable us to tune the porosity by altering the copolymer composition. Subsequently, a PVDF/Ni nanocomposite has been successfully prepared *via* electroless nickel plating. The lamellar nanostructure and the β-crystalline phase, both originating from the block copolymer phase separation, are conserved within the porous template and the nanocomposite. Considering the ferroelectric properties of PVDF and the ferromagnetic behavior of nickel, both nanoporous PVDF and the PVDF/Ni nanocomposite are promising materials for nanotechnological applications. The multiferroic properties of the polymer/nickel nanocomposites will be investigated as part of our ongoing research.

Acknowledgements

This study was funded by the Netherlands Organization for Scientific Research (NWO) *via* a VIDI innovational research grant. The authors are grateful to Gert Alberda van Ekenstein for POM measurements and valuable discussion regarding thermal analysis. We kindly acknowledge Evgeny Polushkin for SEM measurements and Sergey Punzhin for EDX analysis. Beam time on the DUBBLE of ESRF in Grenoble has been made available by NWO, and we thank Wim Bras, Daniel Hermida-Merino and Giuseppe Portale for their experimental assistance.

References

1 H. Kawai, *Jpn. J. Appl. Phys.*, 1969, **8**, 975–976.
2 A. J. Lovinger, *Science*, 1983, **220**, 1115–1121.
3 R. G. Kepler and R. A. Anderson, *Adv. Phys.*, 1992, **41**, 1–57.
4 V. V. Kochervinskii, *Crystallogr. Rep.*, 2003, **48**, 649–675.
5 S. Horiuchi and Y. Tokura, *Nat. Mater.*, 2008, **7**, 357–366.
6 S. B. Lang and S. Muensit, *Appl. Phys. A: Mater. Sci. Process.*, 2006, **85**, 125–134.
7 B. Ameduri, *Chem. Rev.*, 2009, **109**, 6632–6686.
8 L. Priya and J. P. Jog, *J. Polym. Sci., Part B: Polym. Phys.*, 2002, **40**, 1682–1689.
9 D. R. Dillon, K. K. Tenneti, C. Y. Li, F. K. Ko, I. Sics and B. S. Hsiao, *Polymer*, 2006, **47**, 1678–1688.
10 C. W. Nan, M. I. Bichurin, S. X. Dong, D. Viehland and G. Srinivasan, *J. Appl. Phys.*, 2008, **103**, 031101.
11 J. Ma, J. M. Hu, Z. Li and C. W. Nan, *Adv. Mater.*, 2011, **23**, 1062–1087.
12 K. Mori and M. Wuttig, *Appl. Phys. Lett.*, 2002, **81**, 100–101.
13 J. Zhai, S. Dong, Z. Xing, J. Li and D. Viehland, *Appl. Phys. Lett.*, 2006, **89**, 083507.
14 Y. P. Guo, Y. Liu, J. L. Wang, R. L. Withers, H. Chen, L. Jin and P. Smith, *J. Phys. Chem. C*, 2010, **114**, 13861–13866.

15 L. Leibler, *Macromolecules*, 1980, **13**, 1602–1617.
16 F. S. Bates and G. H. Fredrickson, *Annu. Rev. Phys. Chem.*, 1990, **41**, 525–557.
17 A. K. Khandpur, S. Forster, F. S. Bates, I. W. Hamley, A. J. Ryan, W. Bras, K. Almdal and K. Mortensen, *Macromolecules*, 1995, **28**, 8796–8806.
18 I. W. Hamley. *The Physics of Block Copolymers*, Oxford University Press, Oxford, 1998.
19 F. S. Bates and G. H. Fredrickson, *Phys. Today*, 1999, **52**, 32–38.
20 Y. Matsushita, *Macromolecules*, 2007, **40**, 771–776.
21 T. S. Bailey, J. Rzayev and M. A. Hillmyer, *Macromolecules*, 2006, **39**, 8772–8781.
22 D. A. Olson, L. Chen and M. A. Hillmyer, *Chem. Mater.*, 2008, **20**, 869–890.
23 H. Uehara, M. Kakiage, M. Sekiya, D. Sakuma, T. Yamonobe, N. Takano, A. Barraud, E. Meurville and P. Ryser, *ACS Nano*, 2009, **3**, 924–932.
24 L. M. Pitet, M. A. Amendt and M. A. Hillmyer, *J. Am. Chem. Soc.*, 2010, **132**, 8230–8231.
25 E. Drockenmuller, L. Y. T. Li, D. Y. Ryu, E. Harth, T. P. Russell, H. C. Kim and C. J. Hawker, *J. Polym. Sci., Part A: Polym. Chem.*, 2005, **43**, 1028–1037.
26 R. Maki-Ontto, K. de Moel, W. de Odorico, J. Ruokolainen, M. Stamm, G. ten Brinke and O. Ikkala, *Adv. Mater.*, 2001, **13**, 117–121.
27 I. Vukovic, S. Punzhin, Z. Vukovic, P. Onck, J. T. M. De Hosson, G. ten Brinke and K. Loos, *ACS Nano*, 2011, **5**, 6339–6348.
28 V. S. D. Voet, T. E. Pick, S. M. Park, M. Moritz, A. T. Hammack, J. J. Urban, D. F. Ogletree, D. L. Olynick and B. A. Helms, *J. Am. Chem. Soc.*, 2011, **133**, 2812–2815.
29 H. Uehara, T. Yoshida, M. Kakiage, T. Yamanobe, T. Komoto, K. Nomura, K. Nakajima and M. Matsuda, *Macromolecules*, 2006, **39**, 3971–3974.
30 I. Lee, P. T. Hammond and M. F. Rubner, *Chem. Mater.*, 2003, **15**, 4583–4589.
31 Y. Kobayashi, Y. Tadaki, D. Nagao and M. Konno, *J. Phys. Conf. Ser.*, 2007, **61**, 582–586.
32 D. Zabetakis and W. J. Dressick, *ACS Appl. Mater. Interfaces*, 2009, **1**, 4–25.
33 Y. Boontongkong, R. E. Cohen and M. F. Rubner, *Chem. Mater.*, 2000, **12**, 1628–1633.
34 T. Hashimoto, K. Tsutsumi and Y. Funaki, *Langmuir*, 1997, **13**, 6869–6872.
35 T. P. Lodge, *Macromol. Chem. Phys.*, 2003, **204**, 265–273.
36 J. S. Wang and K. Matyjaszewski, *J. Am. Chem. Soc.*, 1995, **117**, 5614–5615.
37 T. E. Patten and K. Matyjaszewski, *Adv. Mater.*, 1998, **10**, 901–915.
38 G. G. du Sart, R. Rachmawati, V. Voet, G. A. van Ekenstein, E. Polushkin, G. ten Brinke and K. Loos, *Macromolecules*, 2008, **41**, 6393–6399.
39 O. W. Webster, *Science*, 1991, **251**, 887–893.
40 K. Matyjaszewski and J. H. Xia, *Chem. Rev.*, 2001, **101**, 2921–2990.
41 M. Destarac, K. Matyjaszewski, E. Silverman, B. Ameduri and B. Boutevin, *Macromolecules*, 2000, **33**, 4613–4615.
42 Z. Q. Shi and S. Holdcroft, *Macromolecules*, 2004, **37**, 2084–2089.
43 Z. Q. Shi and S. Holdcroft, *Macromolecules*, 2005, **38**, 4193–4201.
44 K. Xu, K. Li, P. Khanchaitit and Q. Wang, *Chem. Mater.*, 2007, **19**, 5937–5945.
45 K. Li, S. W. Liang, Y. Y. Lu and Q. Wang, *Macromolecules*, 2007, **40**, 4121–4123.
46 G. Laruelle, E. Nicol, B. Ameduri, J. F. Tassin and N. Ajellal, *J. Polym. Sci., Part A: Polym. Chem.*, 2011, **49**, 3960–3969.
47 H. Schmalz, A. Boker, R. Lange, G. Krausch and V. Abetz, *Macromolecules*, 2001, **34**, 8720–8729.
48 H. Schmalz, A. Knoll, A. J. Muller and V. Abetz, *Macromolecules*, 2002, **35**, 10004–10013.
49 B. Nandan, J. Y. Hsu and H. L. Chen, *Polym. Rev.*, 2006, **46**, 143–172.
50 P. Rangarajan, R. A. Register and L. J. Fetters, *Macromolecules*, 1993, **26**, 4640–4645.
51 Y. L. Loo, R. A. Register and A. J. Ryan, *Macromolecules*, 2002, **35**, 2365–2374.
52 J. Guiot, B. Ameduri and B. Boutevin, *Macromolecules*, 2002, **35**, 8694–8707.
53 M. Pianca, E. Barchiesi, G. Esposto and S. Radice, *J. Fluorine Chem.*, 1999, **95**, 71–84.
54 C. Marega and A. Marigo, *Eur. Polym. J.*, 2003, **39**, 1713–1720.
55 C. R. Herrero, E. Morales and J. L. Acosta, *J. Appl. Polym. Sci.*, 1994, **51**, 1189–1197.
56 C. Delrio and J. L. Acosta, *Polym. Int.*, 1994, **34**, 417–424.
57 F. Guo, K. Jankova, L. Schulte, M. E. Vigild and S. Ndoni, *Macromolecules*, 2008, **41**, 1486–1493.
58 E. N. Dalal, *Langmuir*, 1987, **3**, 1009–1015.
59 W. Eerenstein, N. D. Mathur and J. F. Scott, *Nature*, 2006, **442**, 759–765.

